

Automatic Label Correction for the Accurate Edge Detection of Overlapping Cervical Cells

Jiawei Liu , *Student Member, IEEE*, Qiang Wang, Huijie Fan, *Member, IEEE*, Shuai Wang, Wentao Li, Yandong Tang, *Member, IEEE*, Danbo Wang, Mingyi Zhou, Li Chen

Abstract—Accurate labeling is essential for supervised deep learning methods. In this paper, to accurately segment images of multiple overlapping cervical cells with deep learning models, we propose an automatic label correction algorithm to improve the edge positioning accuracy of overlapping cervical cells in manual labeling. Our algorithm is designed based on gradient guidance, and can automatically correct edge positions for overlapping cervical cells and differences among manual labeling with different annotators. Using the proposed algorithm, we constructed an open cervical cell edge detection dataset (CCEDD) with high labeling accuracy. The experiments on the dataset for training show that our automatic label correction algorithm can improve the accuracy of manual labels and further improve the positioning accuracy of overlapping cells with deep learning models. We have released the dataset and code at <https://github.com/nachifur/automatic-label-correction-CCEDD>.

Index Terms—Label correction, edge detection, cervical cell dataset, overlapping cells, deep learning.

I. INTRODUCTION

CERVICAL cancer ranks fourth in both incidence and mortality among females in the world. It was estimated that there were 570,000 cases and 311,000 deaths of the disease worldwide in 2018 [1]. Cervical cancer is preventable and can be cured in the early stage, as it can be largely detected by cytological screening combined with human papillomavirus virus (HPV) testing. The Papanicolaou test is the most common technique used for early screening

This work is supported by the National Natural Science Foundation of China (61873259, 62073205, 61821005), the Key Research and Development Program of Liaoning (2018225037), and the Youth Innovation Promotion Association of Chinese Academy of Sciences (2019203). (Co-corresponding authors: Huijie Fan; Danbo Wang.)

J. Liu is with State Key Laboratory of Robotics, Shenyang Institute of Automation, Chinese Academy of Sciences, Shenyang, 110016, China; Institutes for Robotics and Intelligent Manufacturing, Chinese Academy of Sciences, Shenyang, 110016, China; College of Robotics and Intelligent Manufacturing, University of Chinese Academy of Sciences, Beijing, 100049, China (email: liujiawei@sia.cn).

H. Fan, W. Li and Y. Tang are with State Key Laboratory of Robotics, Shenyang Institute of Automation, Chinese Academy of Sciences, Shenyang, 110016, China; Institutes for Robotics and Intelligent Manufacturing, Chinese Academy of Sciences, Shenyang, 110016, China (email: fanhuijie@sia.cn).

Q. Wang is with the Key Laboratory of Manufacturing Industrial Integrated, Shenyang University; the State Key Laboratory of Robotics, Shenyang Institute of Automation, Chinese Academy of Sciences, Shenyang, 110016, China (e-mail: wangqiang@sia.cn).

S. Wang is with School of Mechanical Electrical and Information Engineering, Shandong University, Weihai 264209, China (email: shuaiwang@sdu.edu.cn).

D. Wang, M. Zhou and L. Chen are with Department of Gynecology, Cancer Hospital of China Medical University, Shenyang, 110122, China; Liaoning Cancer Hospital and Institute, Shenyang, 110042, China. (email: wangdb@sj-hospital.org).

and diagnosis of cervical cancer. The diagnostic procedure requires a cytologist or pathologist to locate abnormal cells from countless normal cells under the microscope, which is very tedious, labor intensive and highly subjective to human errors [2]. Compared with manual analysis, automatic Papanicolaou smear analysis can reduce time and improve the accuracy of slide inspection by a cytologist. For an automatic Papanicolaou smear analysis system, accurate cell segmentation is essential. However, overlapping clumps of cervical cells often cause false segmentation and affect the slide examination in cervical cell image analysis. Accurate and automatic segmentation of overlapping and small cells is still an essential problem in cervical cell image analysis.

For cytoplasm and nucleus segmentation, some traditional techniques, such as watersheds, active contours and level sets, are widely applied [3], [4], [5], [6], [7]. Recently, Saha *et al.* [8] proposed a cervical nucleus segmentation framework. It generates superpixels through a statistical region merging (SRM) algorithm, and fuses the superpixels using paired region contrast and gradient boundaries. Tareef *et al.* [7] introduced a fast multiwatershed pass method to segment the cell nuclei through one watershed pass utilizing the intensity gradient information and segment the cytoplasm through two watershed passes. Song *et al.* [9] presented an approach that leverages more shape constraints through joint shape template matching for segmenting overlapping cytoplasm of cells. In their other work, under the a priori guidance of the modeled shape, a constrained polymorphism evolution method is used to evolve the shape of each cytoplasm while segmenting all overlapping cytoplasm in the clump [10]. Although all these methods have achieved relatively good segmentation results, they sometime fail in highly overlapping cytoplasm nuclei, noisy background and uneven illumination.

With advances in computational power, deep learning has been applied for cervical cell segmentation [11], [12], [13]. [14] proposed a two-stage cellular segmentation framework. In the framework, the first step is to identify the region of interest by cell detection. Then, the detection result is used as the input for subsequent cytoplasmic segmentation. Zhang *et al.* [15] proposed attention U-Net and graph-based random walk to segment the cell nucleus and cytoplasm. In their work, U-Net is used twice: one predicts the nuclei, and another predicts the cytoplasm edge after polar coordinate sampling.

Using deep learning-based methods can improve the accuracy and robustness of cytoplasm and nuclear segmentation. However, the premise of supervised deep learning methods requires a rich data set and accurate annotations. Currently,

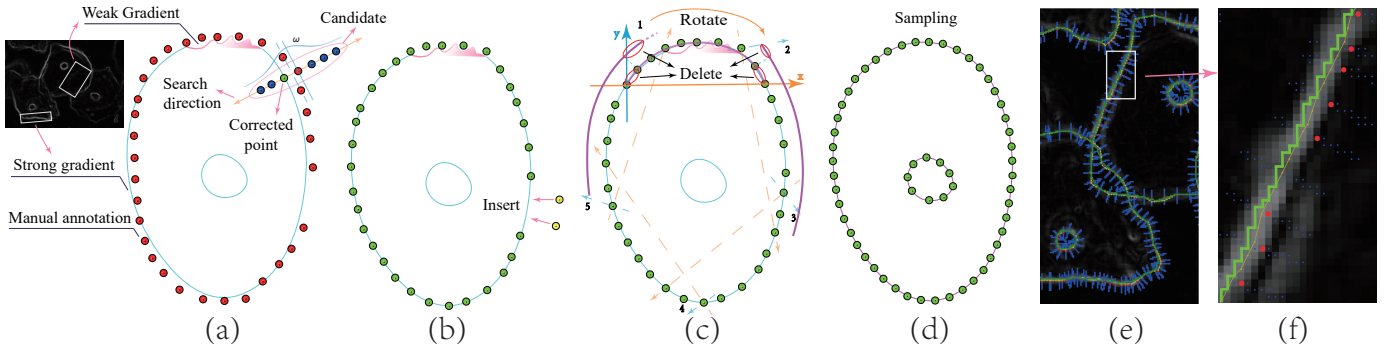


Fig. 1: Workflow of the presented automatic label correction algorithm. (a) label point correction (the red points \rightarrow the green points); (b) interpolation in large gap (the yellow points); (c) smooth edge curve generation (the purple curve); (d) curve sampling; (e) the gradient image with the corrected edges (the green edges); (f) magnification of the gradient image. The whole process is to generate green edges from red points in (f).

cytoplasmic and nuclear segmentation datasets include Shenzhen University dataset [16], Beihang University dataset [14] and ISBI 2015 challenge dataset [17]. The only public dataset, the ISBI Challenge dataset, has a small amount of data and simple image types. The small amount of ISBI data makes it difficult to apply deep learning to cervical cell segmentation.

Medical image datasets are generally annotated by professional physicians. However, labeling medical images is time consuming and labor intensive. One main problem is that even if the label standard is unified, it is still difficult to guarantee the edge positioning accuracy of manual labels. In addition, differences between different annotators are inevitable. At present, most label correction works are concentrated on the semi-supervised training process [18], and there are also some applications in annotations via crowdsourcing [19], [20], classification [21], [22], [23], [24] and natural language processing [25]. Northcutt *et al.* [26] found that label errors in the test sets are numerous and universal: the average error rate in 10 datasets is 3.4%. They find that if the error rate of test labels only increases by 6%, ResNet-18 outperforms ResNet-50 on ImageNet [27] with corrected labels. This indicates that the wrong label will seriously affect the accuracy of the model evaluation. The deployed model for computer-aided diagnosis is selected from many candidate models through model evaluation. The accuracy of the evaluation determines whether the optimal model can be selected, which may affect an accurate diagnosis by the doctor. Therefore, the automatic correction algorithm based on manual labeling is valuable for correcting the errors of manual labeling to generate uniform and accurate annotations.

For accurate edge detection of overlapping cervical cells, we construct a cervical cell image dataset, namely, CCEDD, which contains 686 images with multiple complex types of cervical cells and accurately labeled images. CCEDD can basically satisfy the training of supervised deep learning models in terms of quantity and richness. To eliminate the influence of edge positioning errors and differences between annotators in manual annotation, we proposed a method for automatically correcting labels to generate higher-quality annotated images based on manual labeling. Experiments on some state-of-the-

art deep learning models validate our method and CCEDD dataset.

Our main contributions are summarized as follows:

- We proposed an automatic label correction method for edge detection and image segmentation. By using our corrected label, 7% AP improvement in multiple baseline deep learning models can be observed.
- By using our automatic label correction algorithm, we constructed a larger public cervical cytoplasmic and nuclear edge detection dataset with higher labeling accuracy, which contains 686 annotated images with a resolution of 2048×1536 pixels.

II. AUTOMATIC LABEL CORRECTION

Our proposed label correction algorithm contains four parts: label point correction based on gradient, interpolation in a large gap, smooth edge curve generation based on fusion of the piecewise curve using improving local linear fitting and curve sampling, as shown in Fig. 1. $I(x, y)$ is a cervical cell image, and $g(x, y)$ is the gradient image after smoothing through the Gaussian filter. We denote (x_i, y_i) as x_s^i , which is an original labeled point in $I(x, y)$ by manual annotation. First, we process label point correction as shown in (a), and $\{x_s^i\} \rightarrow \{x_c^i\}$, $i \in \{1, 2, \dots, n_s\}$. Second, we insert extra points in a large gap, as shown in (b), and $\{x_c^i\} \rightarrow \{x_I^j\}$, $j \in \{1, 2, \dots, n_I\}$. n_s and n_I are the number of points before and after interpolation, respectively. Third, we divide the point set $\{x_I^j\}$ into n_c groups. Each set of points is expressed as Φ_k . We use an improved local linear method to fit the curve C_k on Φ_k , $k \in \{1, 2, \dots, n_c\}$. The set of curves $\{C_k\}$ is spliced into a closed curve C_c as shown in (c). Finally, we sample C_c to obtain discrete edges with connectivity C_d as shown in (d).

A. Label Point Correction

Although the annotations are provided by professional doctors, due to human error, the label points usually deviate from the gradient edge. To solve this problem, we designed

a label point correction method based on gradient guidance. To eliminate human error to the greatest extent, retain the originally correct label information and generate accurate labels, we correct the label points only in the strong gradient region, while retaining the original label points in the weak edge region. Our label point correction consists of three steps as follows:

- 1) Detecting whether the position of each mutual label point is in the strong gradient region.
- 2) Determining the candidate point set.
- 3) Correcting the candidate point to a new position with the local largest gradient value.

For an original labeled point x_s^i , we search for the point x_{max}^i with the largest gradient value along the normal direction of the mutual label edge and the search radius is r , which constitutes the candidate point set $\Omega_{x_s^i}$. The corrected label point is x_c^i .

$$x_c^i = \begin{cases} x_{max}^i & \text{if } \Delta > 0 \\ x_s^i & \text{otherwise} \end{cases} \quad (1)$$

where

$$\Delta = \left| \max(\omega_j \cdot g(x_{s_j}^i)) - \min(\omega_j \cdot g(x_{s_j}^i)) \right| - \lambda_t \cdot \max(\omega_j). \quad (2)$$

$x_{s_j}^i$ is a candidate point in $\Omega_{x_s^i}$. We judge whether a point x_s^i is in the strong gradient region through Δ . If $\Delta > 0$, the original labeled point x_s^i needs to be corrected; otherwise, no correction is required. To be robust against image noise, the gradient value of the candidate point $g(x_{s_j}^i)$ is weighted by ω_j . We compute the weight as

$$\omega_j = \kappa_h \left(\left\| x_{s_j}^i - x_s^i \right\|_2 \right), \quad (3)$$

where

$$\kappa_h(\cdot) = \kappa(\cdot/h)/h. \quad (4)$$

κ_h is a weighted kernel function, and the bandwidth is h . $\kappa(x)$ is a Gaussian function with zero mean and one variance. We empirically set the parameters $r = 7, h = r/2, \lambda_t = 20$. After label point correction, $\{x_s^i\} \rightarrow \{x_c^i\}$.

B. Smooth Edge Curve Generation

Due to noise, the edges generated directly by the corrected points $\{x_c^i\}$ are not smooth, so we consider obtaining smooth edges by fitting. We divide a closed curve into several segments and fit each segment separately based on improved local linear fitting to generate smooth cell edge curves.

Interpolation: In the labeling process, we observed that to accurately and quickly outline the geometry of the cells, the annotators densely label the points with large curvature and sparsely label the places with small curvature. We assume that linear fitting can be used on sparsely labeled points. We perform linear interpolation on larger intervals before curve fitting. First, the sparse label point pairs $\{(x_c^i, x_c^r) \mid \|x_c^i - x_c^r\|_2 > 2 \cdot \text{step}\}$. $i = 1, 2 \dots n_s$. $i_r = (i+1)$ if $(i < n_s)$ else 0 are selected. Second, we interpolate between pairs of sparse points to satisfy $\|x_I^j - x_I^r\|_2 < \text{step}$.

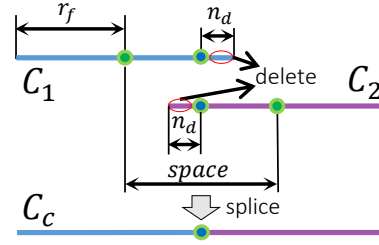


Fig. 2: Splicing multiple curves into one curve.

step is the maximum interval between points after interpolation. $j = 1, 2 \dots n_I$. $j_r = (j+1)$ if $(i < n_I)$ else 0. After interpolation, $\{x_c^i\} \rightarrow \{x_I^j\}$.

Closed Curve Generation: We divide a set of labeled points $\{x_I^j\}$ corresponding to a closed edge into n_c groups. $j \in \{1, 2, \dots, n_I\}$. The number of points in each group n_g is odd. The radius of each group is $r_f = \lfloor (n_g - 1)/2 \rfloor$. $n_c = \lceil n_I / \text{space} \rceil$. The interval of each group center point is $\text{space} = 2 \cdot (r_f - n_d)$ as shown in Fig. 2. The overlapping length of adjacent curves is $2n_d$ to reduce the fitting error of boundary points. In the last curve fitting process, the number of repeated points is $n_r = \text{space} \cdot n_c - n_I$. Each set of points is expressed as $\Phi_k = \{x_I^{i_c}, x_I^{i_c+1}, \dots, x_I^{i_c+2 \cdot r_f - n_r}\}$. $i_c = (k-1) \cdot \text{space} + 1, 1 \leq k \leq n_c$.

In each set of points, the straight line passing through the point $x_I^{i_c}$ and the point $x_I^{i_c+2 \cdot r_f - n_r}$ is used as the x-axis, and the point $x_I^{i_c}$ is used as the origin to establish a new plane rectangular coordinate system. After coordinate transformation, the sets of points $\Phi_k \rightarrow \Phi_k^r$. We generate a curve C_k using local linear weighted fitting on Φ_k^r . This is equivalent to solving the following problem at the target point x .

$$\min_{\beta_0(x), \beta_1(x)} \sum_{j=i_c}^{i_c+2 \cdot r_f - n_r} \omega_j(x) (y_j - \beta_0(x) - \beta_1(x) \cdot x_j) \quad (5)$$

(x_j, y_j) denotes the coordinates of point x_I^j . The weight function is

$$\omega_j(x) = \kappa_h^c(x - x_j) / \sum_{m=i_c}^{i_c+2 \cdot r_f - n_r} \kappa_h^c(x - x_m). \quad (6)$$

The improved kernel function is

$$\kappa_h^c(x - x_m) = \begin{cases} 1.5 \cdot \max \left\{ \left\{ \kappa_h(x - x_m) \right\}_{m=i_c}^{i_c+2 \cdot r_f - n_r} \right\} & \text{if} \\ m = i_c + \lfloor n_d \rfloor \text{ or } m = i_c + 2 \cdot r_f - n_r - \lfloor n_d \rfloor & \\ \kappa_h(x - x_m) & \text{otherwise.} \end{cases} \quad (7)$$

We increase the weight of the point $x_I^{i_c + \lfloor n_d \rfloor}$ and the point $x_I^{i_c + 2 \cdot r_f - n_r - \lfloor n_d \rfloor}$ so that the adjacent curves are connected. The above parameter solution is expressed by a matrix as

$$\beta = (X^T \omega X)^{-1} X^T \omega Y, \quad (8)$$

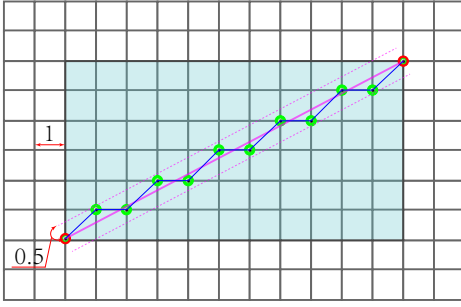


Fig. 3: Generate discrete connected edges from points. The label points are denoted as red points. Discrete edges are composed of green points.

$$\text{in which } X = \begin{bmatrix} 1 & x_{i_c} \\ 1 & x_{i_c+1} \\ \vdots & \vdots \\ 1 & x_{i_c+2 \cdot r_f - n_r} \end{bmatrix}, Y = \begin{bmatrix} y_{i_c} \\ y_{i_c+1} \\ \vdots \\ y_{i_c+2 \cdot r_f - n_r} \end{bmatrix}, \beta = \begin{bmatrix} \beta_0(x) \\ \beta_1(x) \end{bmatrix}, \omega = \begin{bmatrix} \omega_{i_c}(x) & & & \\ & \omega_{i_c+1}(x) & & \\ & & \ddots & \\ & & & \omega_{i_c+2 \cdot r_f - n_r}(x) \end{bmatrix}.$$

We stitch $\{C_k\}$ curves into a closed curve C_c and sample on the interval $[x_I^{i_c+[n_d]}, x_I^{i_c+2 \cdot r_f - n_r - [n_d]}]$. Then, we convert the coordinates of the sampling point to the original coordinate system. Finally, we can obtain discrete edges with connectivity C_d .

Bandwidth Selection: Ghanem and Zhang [28] chose $h = a \times b$ and used $b = 2\sigma n^{1/2}$ proposed in the bandwidth selection guide [29]. In the paper, we adopt $h = a \times b + c$ for edge fitting. For cytoplasm edge fitting, $n_g = \max(\lfloor \text{step} \cdot n_I / 40 \rfloor, 7)$, $a = 10$. For nucleus edge fitting, $n_g = \max(\lfloor \text{step} \cdot n_I / 10 \rfloor, 3)$, $a = 5$. $b = 2\sigma_k n_g^{1/2}$, $c = \lfloor \text{step} \cdot n_g \rfloor / 6$. σ_k is the standard deviation of the ordinate on Φ_k^r .

Smooth Closed Curve: When r_f is fixed, if $space$ is smaller, then n_d is larger, the number of curve segments used to stitch a closed curve is larger, and it is smoother at the nodes of the curve segment. If $n_d = r_f - 0.5$, then $space = 1$ and $n_c = n_I$. We fit a curve C_j at each point in the set $\{x_I^j\}$. We do not sample on the interval $[x_I^{i_c+[n_d]}, x_I^{i_c+2 \cdot r_f - n_r - [n_d]}]$, but only sample at the point x_I^j . In other words, only the position of points is adjusted by curve fitting, and the number of points is not changed by sampling. Because no curves are spliced, the curve C_c is smooth at each point. The sampling point interval can be adjusted by $step$. The smaller the $step$ is, the denser the sampling points of the curve. Considering that the digital image is discrete, we set $step = 1$.

C. Comparison with the Original Label

We successively connect the label points to a closed polygon and perform discrete sampling to obtain edges (Fig. 3). We use this method to generate the original label. It takes 38 s to generate 100 original edge labels from annotated points with

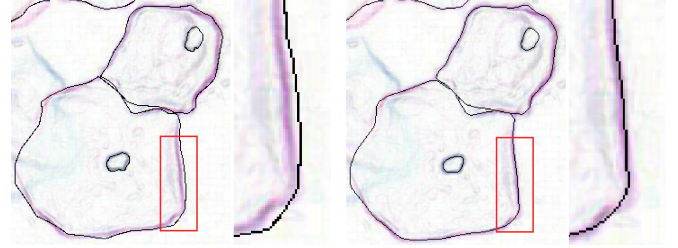


Fig. 4: Label correction results. Original label (left). Corrected label (right).

a size of 2048×1536 pixels on a CPU. Our automatic label correction algorithm takes 270 s to generate corrected edge labels under the same test conditions. Because our corrected label is generated offline and does not affect the neural network model inference time, we have not further optimized it. If the algorithm runs on a GPU, the speed can be further improved, which can save more time for the correction of very large-scale datasets. Fig. 4 is a comparison of the original label and corrected label.

III. EXPERIMENTAL DESIGN

To verify the effectiveness of the label correction method, we evaluated the performance of various models on CCEDD. We uniformly use PyTorch as a deep learning framework. In each experiment, only the model structure and loss function are different, and the training methods and hyperparameter settings are the same. All experiments of this paper are executed on an Intel(R) Xeon(R) Silver 4110 CPU (8 cores, 16 threads, 32 GB memory) and a NVIDIA TITAN V GPU with 12 GB memory.

A. Data Description

We compared CCEDD with other cervical cytology datasets in Table I. CCEDD contains 686 scanned cervical cytology images between 2016 and 2017 from the Liaoning Cancer Hospital & Institute. All of the cases are anonymized. For negative and positive cervical cancer patients with $100 \times$ and $400 \times$ optical magnifications, digital imaging was performed with a Nikon ELIPSE Ci slide scanner, SmartV350D lens and 3 million pixel digital camera. CCEDD includes 686 cervical images with a size of 2048×1536 pixels (Table II). Six expert cytologists delineated the closed cytoplasm and nucleus contours in the cytological images using the labelme annotation tool [30]. In order to ensure the reliability of the test results, we divided the dataset by random shuffle into training set, validation set and test set according to a ratio of 6:1:3. We cut an image with a size of 2048×1536 into 49 image patches with a size of 512×384 pixels (Fig. 5). The actual image resolution is 256×192 for training.

B. Data Augmentation

Augmentor [31] supports multiple image augmentation and randomized elastic distortions. We use the Augmentor software package for data augmentation. The CCEDD consists of

TABLE I: The properties of cervical cytology datasets.

Dataset	Image size	dataset size	Open
ISBI 2014+2015 [17]	1024 × 1024	17	✓
BHU Dataset [14]	512 × 512	580	×
SZU Dataset [16]	1360 × 1024	21	×
CCEDD	2048 × 1536	686	✓

TABLE II: The detailed description of CCEDD.

Dataset	Image size	dataset size	training set size	validation set size	test set size
Uncut CCEDD	2048 × 1536	686	411	68	207
Cut CCEDD	512 × 384	33614	20139	3332	10143

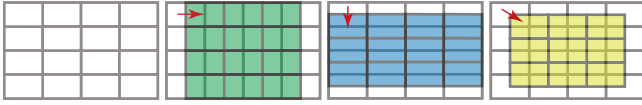


Fig. 5: Image cutting method. 4×4 cutting, 4×3 right offset cutting, 3×4 lower offset cutting, 3×3 right and lower offset cutting.

RGB images. Therefore, we implemented brightness, contrast, hue, saturation adjustment, affine transformation and elastic deformation for training.

C. Baseline Model

Our baseline detectors are RCF [32], UNet [33] and ENDE [34], [35]. RCF is an advanced edge detector in natural images. UNet is a symmetrical encoding and decoding network using short connections and has achieved outstanding success in medical image segmentation [36], [37], [38]. ENDE is an encoding and decoding structure with no skip connection. The bottleneck layer of ENDE uses four residual blocks. We add a layer of regular convolution before dilated convolution with a dilation factor of two in ENDE.

D. Evaluation Metrics

Edge detection accuracy is evaluated using three standard measures: ODS (the best $F = \frac{2 \cdot \text{precision} \cdot \text{recall}}{\text{precision} + \text{recall}}$ for a fixed scale), OIS (the F for the best scale in each image), and AP (the average precision: the area under the precision-recall curve) [39]. We rewrite the evaluation code [39] for fast evaluation on a GPU. On the benchmark model ENDE, the test set (10143 images with a size of 256×192 pixels) with an average FPS of **172** is evaluated. An image of BSD500 [39] is annotated by six persons, while an image in our dataset is annotated by one person. We simplified the evaluation code, which is only suitable for an image with a label, not an image with multiple labels.

E. Training and Parameter Setting

To more accurately evaluate the performance of different models and solve overfitting and underfitting, we choose to

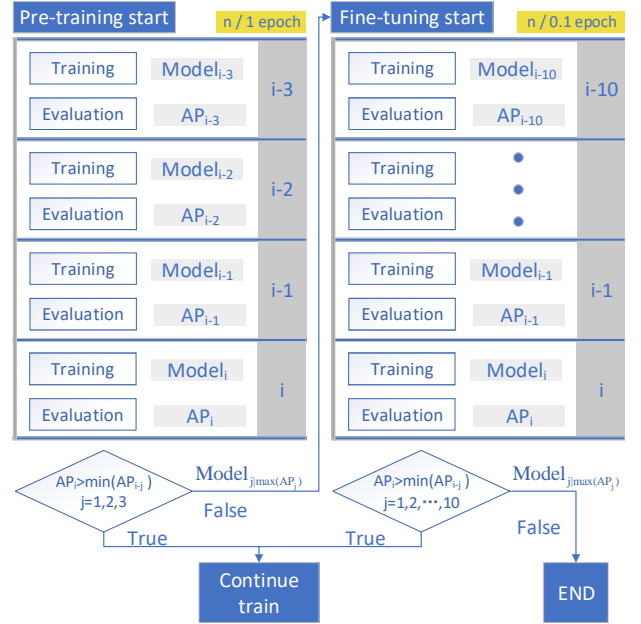


Fig. 6: Training process. Data augmentation in pre-training. No data augmentation in fine-tuning.

adaptively adjust the number of iterations instead of using a fixed number of iterations. Relying on our fast evaluation code, we can obtain the AP of the validation set during the training process to adaptively control the learning rate and the number of iterations.

In the training process, using data augmentation can improve the generalization of the model [31]. To perform rotation and shear operations for data augmentation in the training, zero pixels need to be filled around the image. However, there is no zero pixel padding around the image during the test process. The differences in the distribution between the training set and the test set causes the accuracy of the model on the test set to decrease. Therefore, we only perform data augmentation in pre-training and not in fine-tuning.

The learning rate of networks and the number of training iterations are dynamically adjusted as shown in Fig. 6. The learning rate lr decays from 1^{-4} to 1^{-5} . The maximum number of training iterations is 50 epochs for pre-training and

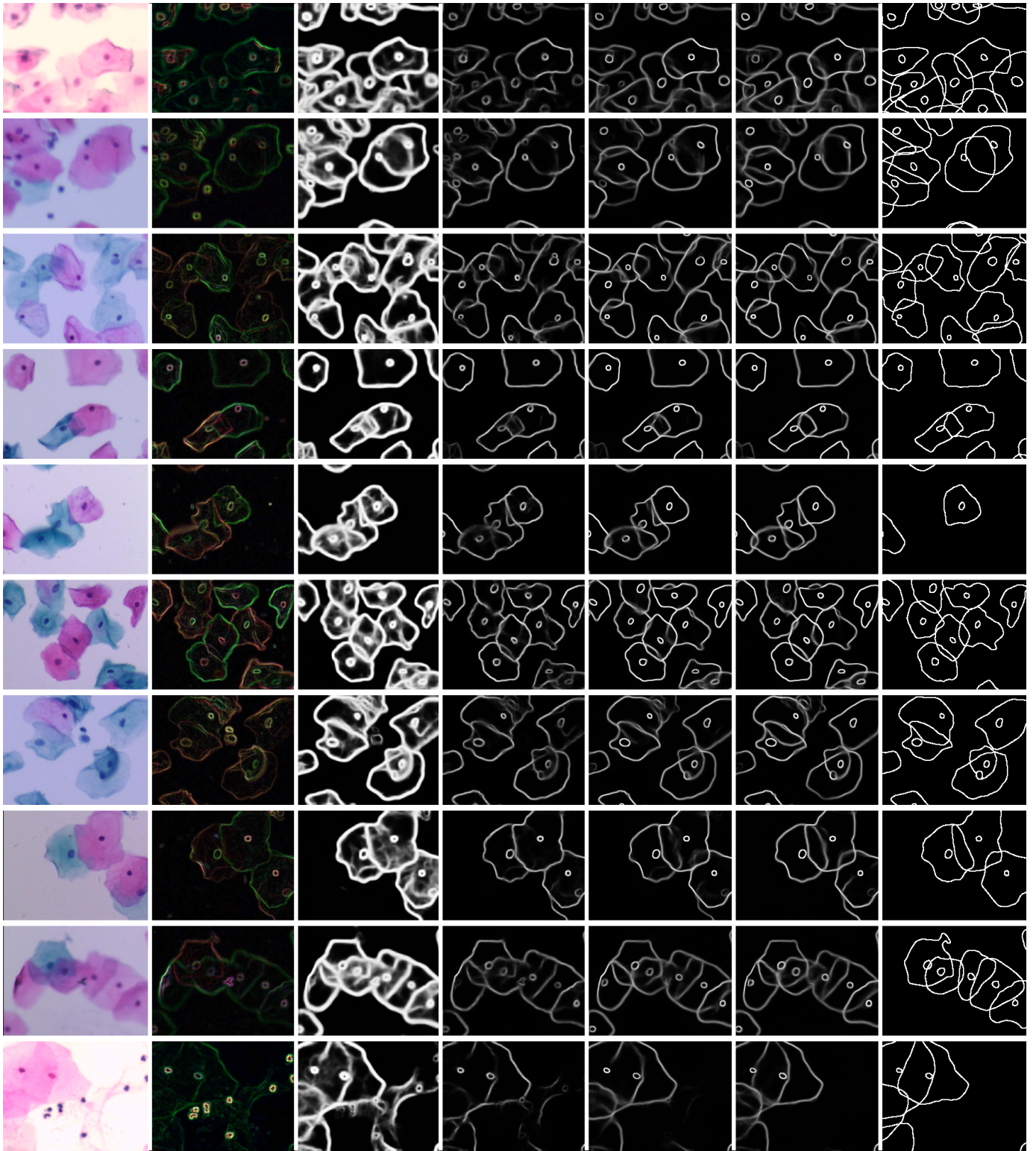


Fig. 7: Edge detection results on CCEDD dataset. From left to right: Original images, RCF + RCFLoss, RCF + BCELoss, UNet + BCELoss, ENDE + BCELoss, Corrected label.

TABLE III: Comparison of different training methods using ENDE and BCELoss on the corrected label.

Training methods	AP	ODS	OIS
w/o augmentation, w/o fine-tuning	0.582	0.566	0.569
w/ augmentation, w/o fine-tuning	0.607	0.583	0.588
w/ augmentation, w/ fine-tuning	0.614	0.588	0.593

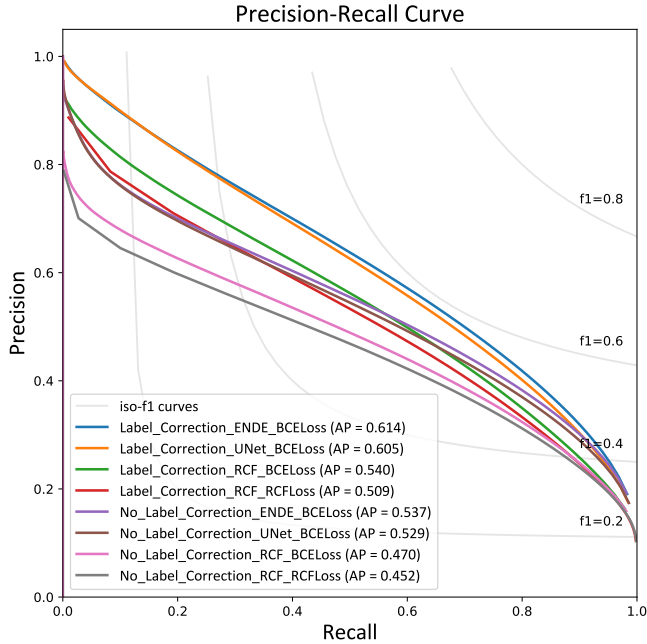


Fig. 8: Evaluation of edge detection algorithms on the CCEDD dataset.

fine-tuning. The period of model evaluation is 1 epoch for pre-training and 0.1 epoch for fine-tuning. We can obtain $Model_i$ and AP_i after the i -th model evaluation. $i = 1, 2, \dots, 50$. If $AP_i < AP_{i-1}$, we automatically adjust the learning rate: $lr_i = 0.5 \cdot lr_{i-1}$. If $AP_i < \min(AP_{i-j})$, the training ends, and we can obtain the optimal model $Model_j | \max(AP_j)$. $j = 1, 2, 3$ in pre-training and $j = 1, 2, \dots, 10$ in fine-tuning. The model is optimized using Adam optimizer with $\beta_1 = 0$ and $\beta_2 = 0.9$ [40].

IV. EXPERIMENTAL RESULTS AND DISCUSSION

A. Ablation Study for Training Methods

Using data augmentation leads to differences in the distribution between the training set and the test set. This may decrease the accuracy of the model on the test set. Table III can verify the effectiveness of our training method, which can lead to a 3% AP improvement.

B. Model and Loss Function Comparison

Our baseline detectors are RCF [32], UNet [33] and ENDE. We use the original label and the corrected label to train and test these models. The quantitative measurement is shown in Table IV and Fig. 8. Fig. 7 shows the final detection results on CCEDD. We found that the performances of all models are

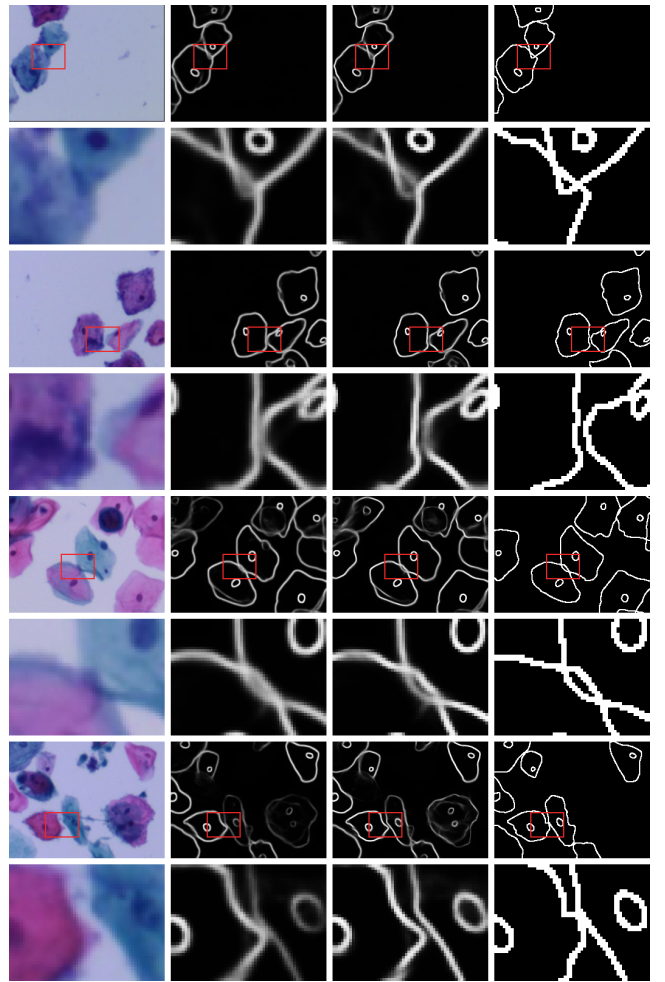


Fig. 9: Compared with the original label, using the corrected label training model can improve the small edge positioning accuracy. From left to right: Original images, ENDE/BCELoss + Original label, ENDE/BCELoss + Corrected label, the corrected labels. Simultaneous magnification of multiple image is provided by [41].

improved by 7 % AP. Although RCF is the most advanced edge detector in natural images, it has the worst performance on CCEDD. At the same time, RCF loss does not apply to CCEDD. Because the RCF model and RCFLoss produce coarser edges with poor positioning accuracy, this may be more robust for natural image edge detection, but it is not suitable for accurate cervical cell edge detection. ENDE has one third of UNet's parameters but obtains the highest accuracy. We think this is because ENDE does not skip connections and does not require a feature fusion layer, so the number of parameters is small. ENDE using dilated convolution can obtain a larger receiving field without downsampling, which achieves higher positioning accuracy.

Compared with the original label, using the corrected label data to train multiple models can improve AP by approximately 7%. Table V shows that AP improvement comes from two aspects. First, in the training process, using the corrected label training model can improve the edge positioning accuracy (Fig. 9, Fig. 10). Second, the corrected label can improve

TABLE IV: Edge detection results on the test set of CCEDD dataset.

Model / Loss	Label correction			No label correction			Params(M)
	AP	ODS	OIS	AP	ODS	OIS	
RCF / RCFLoss	0.509	0.529	0.525	0.452	0.496	0.493	14.81
RCF / BCELoss	0.540	0.545	0.548	0.470	0.508	0.515	
UNet / BCELoss	0.605	0.579	0.584	0.529	0.542	0.549	31.03
ENDE / BCELoss	0.614	0.588	0.593	0.537	0.550	0.557	8.42

TABLE V: Training and evaluation on the original label and the corrected label using ENDE with BCELoss.

Training / Evaluation	AP	ODS	OIS
Original / Original	0.537	0.550	0.557
Original / Corrected	0.574	0.570	0.575
Corrected / Corrected	0.614	0.588	0.593

the evaluation accuracy in the testing process (Table V).

C. Computational Complexity

Our benchmark detection model ENDE is a fast one-stage network with a small amount of parameters. The speed of ENDE is as follows. For 207 images with a resolution of 1024×768 , the average FPS is 8. For 207 images with a resolution of 512×512 , the average FPS is 23. For 10413 images with a resolution of 256×192 , the average FPS is **184**.

Many cervical cell segmentation approaches [6], [5], [7], [14], [15] consist of three stages, including nucleus candidate detection, cell localizations and cytoplasm segmentation. Wan *et al.* [14] tested the speed on a unified platform using images with a resolution of 512×512 . The methods of [14], [3] and [17] took 17.67 s, 35.69 s and 213.62 s per image, respectively.

The speed of ENDE is $400 \times$ faster than that of [14]. We have not tested the speed of the [14] method on a unified platform, but we obviously have a faster speed. This means that using the edge detected by ENDE as a priori input to the cervical cell segmentation network improves performance at a small cost.

V. CONCLUSIONS

We proposed an automatic correction label method that can be used to eliminate the influence of poor edge position accuracy and differences between different annotators in manual annotation. Using our method can generate higher-quality label images. We verify our method on multiple deep learning models. Compared with the original label, using the corrected label to train deep neural networks can lead to a 7% AP improvement. Our training method can eliminate the influence of different distributions of the training set and test set when using data augmentation and lead to a 3% AP improvement.

We can accurately complete the multicell, large-scale overlapping, complex background cytoplasm and nuclear fast edge detection task by training ENDE on CCEDD. ENDE achieves higher accuracy with one-third of the parameters compared to UNet, which means ENDE can be integrated into other cervical cell segmentation models to enhance the segmentation performance with only a small cost.

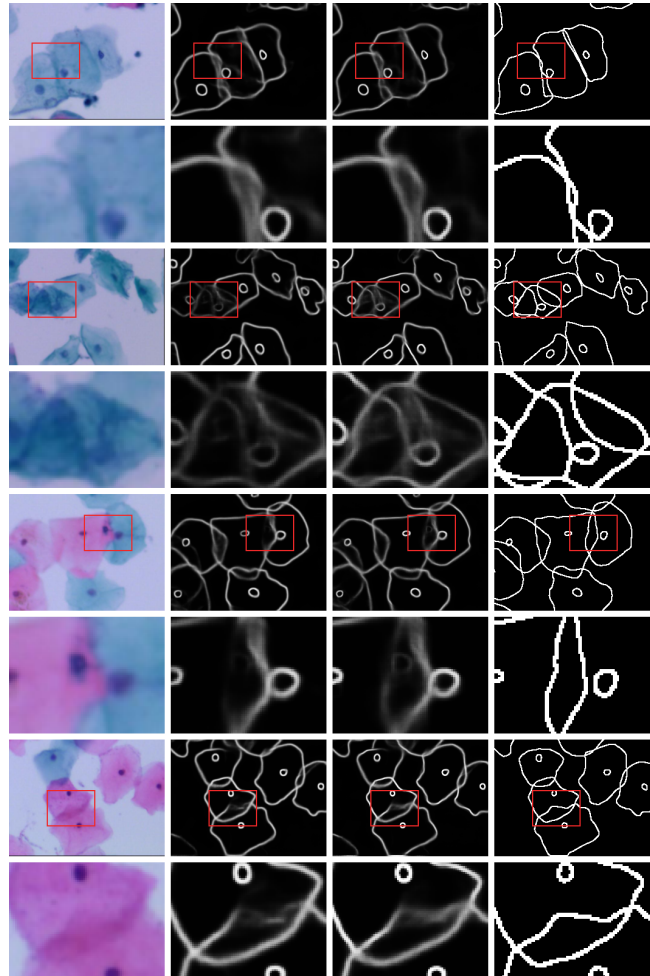


Fig. 10: Compared with the original label, using the corrected label training model can improve the positioning accuracy of overlapping cells. From left to right: Original images, ENDE/BCELoss + Original label, ENDE/BCELoss + Corrected label, the corrected labels. Simultaneous magnification of multiple image is provided by [41].

Our label correction method can be used in the construction of other edge detection and image segmentation datasets to improve the accuracy of annotations. We only conducted experiments on CCEDD to verify the effectiveness of our label correction method, since it is difficult to obtain the original label point of other datasets. In future work, we will use this method to improve the accuracy of other segmentation datasets not limited to CCEDD. At the same time, we plan to develop a method that can improve the quality of annotations without the original annotation points, which will greatly expand the

scope of application.

REFERENCES

- [1] F. Bray, J. Ferlay, I. Soerjomataram, R. L. Siegel, L. A. Torre, and A. Jemal, "Global cancer statistics 2018: Globocan estimates of incidence and mortality worldwide for 36 cancers in 185 countries," *CA: a cancer journal for clinicians*, vol. 68, no. 6, pp. 394–424, 2018.
- [2] W. William, A. Ware, A. H. Basaza-Ejiri, and J. Obungoloch, "A review of image analysis and machine learning techniques for automated cervical cancer screening from pap-smear images," *Computer methods and programs in biomedicine*, vol. 164, pp. 15–22, 2018.
- [3] Z. Lu, G. Carneiro, A. P. Bradley, D. Ushizima, M. S. Nosrati, A. G. Bianchi, C. M. Carneiro, and G. Hamarneh, "Evaluation of three algorithms for the segmentation of overlapping cervical cells," *IEEE journal of biomedical and health informatics*, vol. 21, no. 2, pp. 441–450, 2016.
- [4] A. Marquez-Grajales, H.-G. Acosta-Mesa, E. Mezura-Montes, and R. Hernández-Jiménez, "Cervical image segmentation using active contours and evolutionary programming over temporary acetowhite patterns," in *2016 IEEE Congress on Evolutionary Computation (CEC)*. IEEE, 2016, pp. 3863–3870.
- [5] H. A. Phoulady, D. Goldof, L. O. Hall, and P. R. Mouton, "A framework for nucleus and overlapping cytoplasm segmentation in cervical cytology extended depth of field and volume images," *Computerized Medical Imaging and Graphics*, vol. 59, pp. 38–49, 2017.
- [6] A. Tareef, Y. Song, W. Cai, H. Huang, H. Chang, Y. Wang, M. Fulham, D. Feng, and M. Chen, "Automatic segmentation of overlapping cervical smear cells based on local distinctive features and guided shape deformation," *Neurocomputing*, vol. 221, pp. 94–107, 2017.
- [7] A. Tareef, Y. Song, H. Huang, D. Feng, M. Chen, Y. Wang, and W. Cai, "Multi-pass fast watershed for accurate segmentation of overlapping cervical cells," *IEEE Transactions on Medical Imaging*, vol. 37, no. 9, pp. 2044–2059, 2018.
- [8] R. Saha, M. Bajger, and G. Lee, "Srm superpixel merging framework for precise segmentation of cervical nucleus," in *2019 Digital Image Computing: Techniques and Applications (DICTA)*. IEEE, 2019, pp. 1–8.
- [9] Y. Song, J. Qin, B. Lei, S. He, and K.-S. Choi, "Joint shape matching for overlapping cytoplasm segmentation in cervical smear images," in *2019 IEEE 16th International Symposium on Biomedical Imaging (ISBI 2019)*. IEEE, 2019, pp. 191–194.
- [10] Y. Song, L. Zhu, B. Lei, B. Sheng, Q. Dou, J. Qin, and K.-S. Choi, "Constrained multi-shape evolution for overlapping cytoplasm segmentation," *arXiv preprint arXiv:2004.03892*, 2020.
- [11] Y. Song, L. Zhang, S. Chen, D. Ni, B. Lei, and T. Wang, "Accurate segmentation of cervical cytoplasm and nuclei based on multiscale convolutional network and graph partitioning," *IEEE Transactions on Biomedical Engineering*, vol. 62, no. 10, pp. 2421–2433, 2015.
- [12] A. Tareef, Y. Song, H. Huang, Y. Wang, D. Feng, M. Chen, and W. Cai, "Optimizing the cervix cytological examination based on deep learning and dynamic shape modeling," *Neurocomputing*, vol. 248, pp. 28–40, 2017.
- [13] A. Sarwar, A. A. Sheikh, J. Manhas, and V. Sharma, "Segmentation of cervical cells for automated screening of cervical cancer: a review," *Artificial Intelligence Review*, pp. 1–39, 2019.
- [14] T. Wan, S. Xu, C. Sang, Y. Jin, and Z. Qin, "Accurate segmentation of overlapping cells in cervical cytology with deep convolutional neural networks," *Neurocomputing*, vol. 365, pp. 157–170, 2019.
- [15] H. Zhang, H. Zhu, and X. Ling, "Polar coordinate sampling-based segmentation of overlapping cervical cells using attention u-net and random walk," *Neurocomputing*, vol. 383, pp. 212–223, 2020.
- [16] Y. Song, E.-L. Tan, X. Jiang, J.-Z. Cheng, D. Ni, S. Chen, B. Lei, and T. Wang, "Accurate cervical cell segmentation from overlapping clumps in pap smear images," *IEEE transactions on medical imaging*, vol. 36, no. 1, pp. 288–300, 2016.
- [17] Z. Lu, G. Carneiro, and A. P. Bradley, "An improved joint optimization of multiple level set functions for the segmentation of overlapping cervical cells," *IEEE Transactions on Image Processing*, vol. 24, no. 4, pp. 1261–1272, 2015.
- [18] G. Zheng, A. H. Awadallah, and S. Dumais, "Meta label correction for learning with weak supervision," *arXiv preprint arXiv:1911.03809*, 2019.
- [19] S. Bhadra and M. Hein, "Correction of noisy labels via mutual consistency check," *Neurocomputing*, vol. 160, pp. 34–52, 2015.
- [20] B. Nicholson, V. S. Sheng, and J. Zhang, "Label noise correction and application in crowdsourcing," *Expert Systems with Applications*, vol. 66, pp. 149–162, 2016.
- [21] B. Nicholson, J. Zhang, V. S. Sheng, and Z. Wang, "Label noise correction methods," in *2015 IEEE International Conference on Data Science and Advanced Analytics (DSAA)*. IEEE, 2015, pp. 1–9.
- [22] J. Kremer, F. Sha, and C. Igel, "Robust active label correction," in *International Conference on Artificial Intelligence and Statistics*, 2018, pp. 308–316.
- [23] K. Guo, R. Cao, X. Kui, J. Ma, J. Kang, and T. Chi, "Lcc: towards efficient label completion and correction for supervised medical image learning in smart diagnosis," *Journal of Network and Computer Applications*, vol. 133, pp. 51–59, 2019.
- [24] X. Wang, Y. Hua, E. Kodirov, and N. M. Robertson, "Proselflc: Progressive self label correction for training robust deep neural networks," *arXiv preprint arXiv:2005.03788*, 2020.
- [25] X. Zhu, G. Liu, B. Su, and J. P. Nees, "Dynamic label correction for distant supervision relation extraction via semantic similarity," in *CCF International Conference on Natural Language Processing and Chinese Computing*. Springer, 2019, pp. 16–27.
- [26] C. G. Northcutt, A. Athalye, and J. Mueller, "Pervasive label errors in test sets destabilize machine learning benchmarks," *arXiv preprint arXiv:2103.14749*, 2021.
- [27] J. Deng, W. Dong, R. Socher, L. Li, Kai Li, and Li Fei-Fei, "Imagenet: A large-scale hierarchical image database," in *2009 IEEE Conference on Computer Vision and Pattern Recognition*, 2009, pp. 248–255.
- [28] D. Ghanem and J. Zhang, "'effortless perfection: do chinese cities manipulate air pollution data?'" *Journal of Environmental Economics and Management*, vol. 68, no. 2, pp. 203–225, 2014.
- [29] J. McCrary, "Manipulation of the running variable in the regression discontinuity design: A density test," *Journal of econometrics*, vol. 142, no. 2, pp. 698–714, 2008.
- [30] K. Wada, "labelme: Image Polygonal Annotation with Python," <https://github.com/wkentaro/labelme>, 2016.
- [31] M. D. Bloice, P. M. Roth, and A. Holzinger, "Biomedical image augmentation using augmentor," *Bioinformatics*, vol. 35, no. 21, pp. 4522–4524, 2019.
- [32] Y. Liu, M. Cheng, X. Hu, J. Bian, L. Zhang, X. Bai, and J. Tang, "Richer convolutional features for edge detection," *IEEE Transactions on Pattern Analysis and Machine Intelligence*, vol. 41, no. 8, pp. 1939–1946, 2019.
- [33] O. Ronneberger, P. Fischer, and T. Brox, "U-net: Convolutional networks for biomedical image segmentation," in *International Conference on Medical image computing and computer-assisted intervention*. Springer, 2015, pp. 234–241.
- [34] J. Johnson, A. Alahi, and L. Fei-Fei, "Perceptual losses for real-time style transfer and super-resolution," in *Computer Vision – ECCV 2016*, B. Leibe, J. Matas, N. Sebe, and M. Welling, Eds. Cham: Springer International Publishing, 2016, pp. 694–711.
- [35] K. Nazeri, E. Ng, T. Joseph, F. Qureshi, and M. Ebrahimi, "Edgeconnect: Structure guided image inpainting using edge prediction," in *2019 IEEE/CVF International Conference on Computer Vision Workshop (ICCVW)*, 2019, pp. 3265–3274.
- [36] Y.-X. Zhao, Y.-M. Zhang, M. Song, and C.-L. Liu, "Multi-view semi-supervised 3d whole brain segmentation with a self-ensemble network," in *International Conference on Medical Image Computing and Computer-Assisted Intervention*. Springer, 2019, pp. 256–265.
- [37] B. Lei, Z. Xia, F. Jiang, X. Jiang, Z. Ge, Y. Xu, J. Qin, S. Chen, T. Wang, and S. Wang, "Skin lesion segmentation via generative adversarial networks with dual discriminators," *Medical Image Analysis*, p. 101716, 2020.
- [38] L. Borne, D. Rivière, M. Mancip, and J.-F. Mangin, "Automatic labeling of cortical sulci using patch-or cnn-based segmentation techniques combined with bottom-up geometric constraints," *Medical Image Analysis*, p. 101651, 2020.
- [39] P. Arbelaez, M. Maire, C. Fowlkes, and J. Malik, "Contour detection and hierarchical image segmentation," *IEEE transactions on pattern analysis and machine intelligence*, vol. 33, no. 5, pp. 898–916, 2010.
- [40] D. P. Kingma and J. Ba, "Adam (2014), a method for stochastic optimization," in *Proceedings of the 3rd International Conference on Learning Representations (ICLR)*, *arXiv preprint arXiv*, vol. 1412, 2015.
- [41] J. Liu, "MulimgViewer: A multi-image viewer for image comparison and image stitching," <https://github.com/nachifur/MulimgViewer>, 2020.